RESEARCH PAPER

CrossMark

Load analyses of welded high-strength steel structures using image correlation and diffraction techniques

Dirk Schroepfer [1] · Arne Kromm [1] · Thomas Kannengiesser [1]

Abstract

In an increasing number of modern steel applications, high-strength structural steel grades are demanded to meet specifications regarding a high load-bearing capacity and a low operating weight. Lightweight design rules enhance the safety requirements, especially for welded joints. Besides a higher cracking risk for high-strength steel welds, the formation of tensile residual stresses might lead to fracture due to overloading or premature failure if not adequately considered. In this study, a stress-strain analysis was conducted at component-related structures from S960QL using digital image correlation while preheating, welding and cooling adjacent to the weld seam. X-ray diffraction analysis of the local residual stresses in the weld seam showed a good comparability with global analyses using either a DIC system or a special testing facility, which allowed in situ measurements of welding loads. By analysing two different seam geometries, it could be shown that lower multi-axial stresses arise if a narrower weld groove is used. Comparative analyses revealed a direct correlation of the local residual stresses in the weld with transverse shrinkage restraint, whereas the residual stress level in the HAZ is significantly affected by the bending restraint of the weld construction and the occurring bending stresses, respectively.

Keywords Residual stresses · GMA welding · Restraint · High-strength steels · Process parameters

1 Introduction

The demand for high-strength fine-grained structural steel in modern steel constructions increased in recent years in a growing number of applications in civil engineering and mobile crane manufacturing [1]. This led to a development of numerous high-strength base and filler materials by the steel producers with yield strength from 960 MPa [2]. The economical application of these steels is determined by high safety requirements of the welds among achieving adequate mechanical properties. More challenges in welding are also a result of closer technical boundaries and a higher elastic ratio. In particular, high tensile residual stresses in the welds are able to diminish a component's safety [3]. At highly restrained weld conditions, such as repair

welds or in thick-walled support structures, residual stresses may reach crack critical levels [4] (see Fig. 1). Codes and standards regarding manufacturing and design of welded components assume residual stresses on the amount of the yield strength [6, 7]. The bases of these assumptions are studies, which had been conducted predominantly at free shrinking laboratory samples from mild steels. Component relevant restraints and heat conduction conditions as well as the phase transformation behaviour of high-strength structural steels had rather not been considered. As a rule, the consequence is a highly conservative design of welded constructions. Hence, the economic benefit using high-strength steels is limited. However, recent studies revealed that residual stresses in those welds are lower than the yield strength in general [8–11].

The residual stress state of a welded component is subjected to a complex interaction of the applied material, the restraint condition based on the design and the process conditions as well as the heat control [12]. Using an adequate heat control during welding, a minimisation of the local restraint stresses in the weld seam and of the global reaction forces and stresses due to shoring effects from an external restraint is attainable [8, 9, 13, 14]. Within the scope of an AiF-research project (IGF.-Nr. 17978 N), various kinds of experimental load analyses were conducted [5, 15]. It was aspired to

---

✉ Dirk Schroepfer
  dirk.schroepfer@bam.de

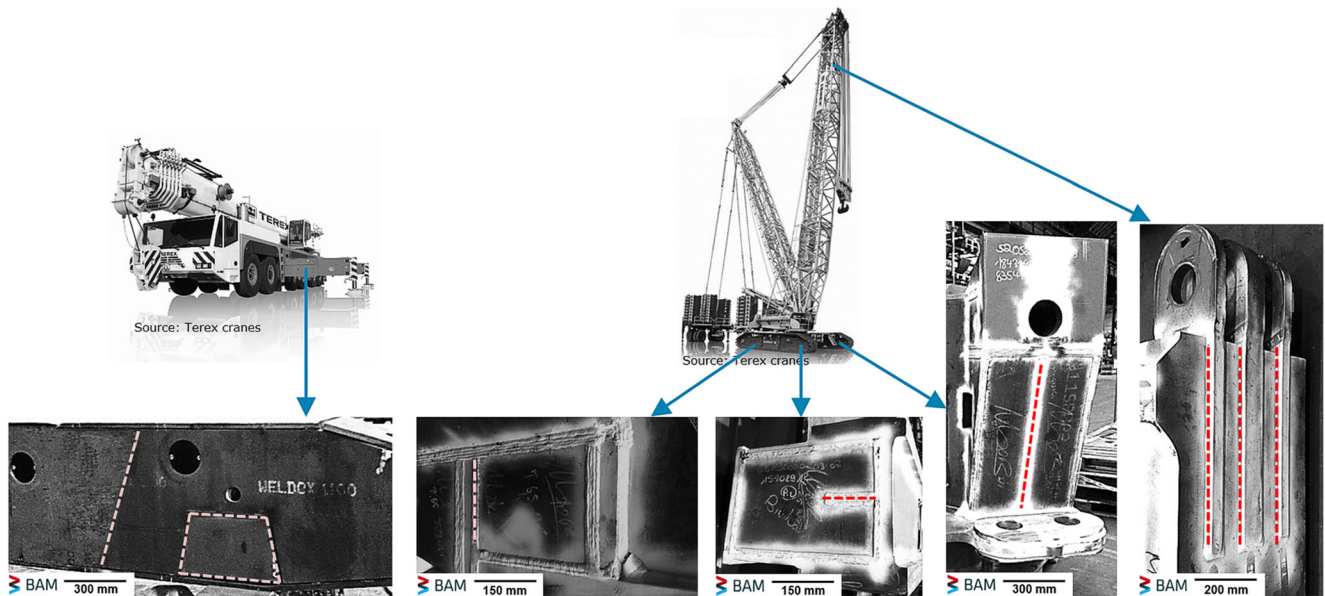[1] Bundesanstalt für Materialforschung und -prüfung (BAM), Unter den Eichen 87, 12205 Berlin, Germany

Fig. 1 Examples of typical weld seams with high restraints in mobile crane fabrication [5]

examine the welding process regarding the produced welding loads and stresses. For this purpose, the transfer of restraint conditions of real welded structures to welding experiments in bench-scale models is mandatory [16, 17]. Therefore, massive slot specimens of high-strength steel S960QL were used (see Fig. 2).

2 Experimental

2.1 Restraint condition

These slot specimens as compact self-restraining structures exhibit realistic conditions in terms of heat conduction and shoring

effects. To compare restraint conditions of different weld constructions, the restraint intensity concept was established by Satoh [18]. The restraint intensity transverse to the weld R_{Fy} is the spring rigidity of the surrounding structure towards the weld seam based on the seam length L_S. The specimen was experimentally and numerically analysed to determine the restraint intensity transverse to the weld direction.

For the experimental analyses, the slot of the weld seam was expanded using a hydraulic spreader. A defined load of $F_y = 115$ kN was applied at three various positions of the slot (see Fig. 2a). In the course of this, a digital image correlation (DIC) system was used to measure the displacement in the surrounding area of the slot (see Fig. 2b).
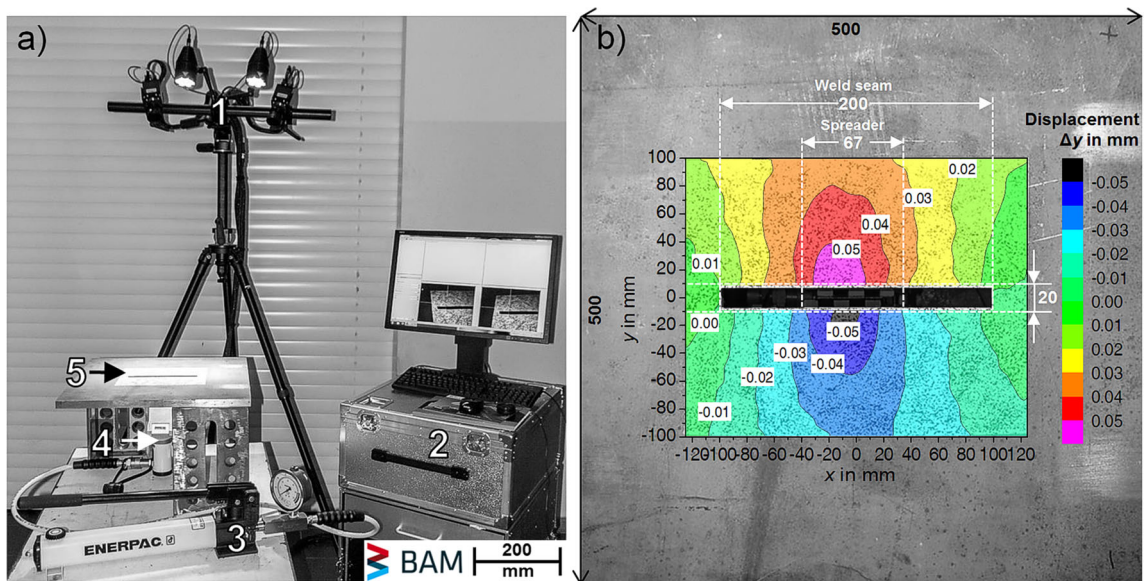

Fig. 2 Experimental determination of restraint intensity of the slot specimen: **a** test setup (1 stereo camera system, 2 DIC-system (Aramis), 3 hydraulic pump, 4 spreader, 5 specimen); **b** displacement in the analysed area due to loading during restraint intensity determination as per [5]

Fig. 3 Numerical determination of restraint intensity of the slot specimen: **a** displacement in the analysed area due to loading; **b** analysed seam geometries as per [5]
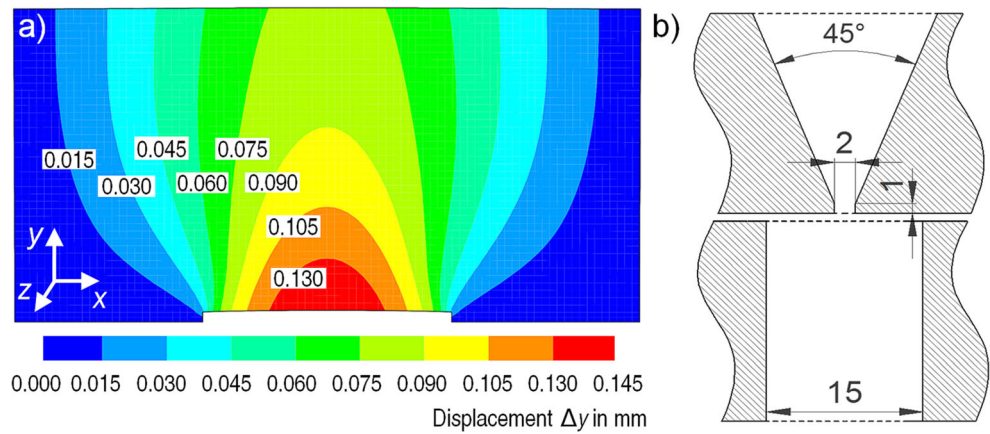
The numerical determination of the restraint intensity was performed by means of FE calculation. Therefore, a solid model of the slot specimen was created and meshed. In the FE calculation, a distributed load of $p = 100$ N mm^{-2} was applied on the fusion face transverse to the weld seam and the displacement was calculated (see Fig. 3a). This analysis was conducted for a square weld according to experimental determination and for a V-type weld (see Fig. 3b).

Both methods the experimental and the numerical analysis revealed qualitatively and quantitatively similar strain fields in the vicinity of the weld with increasing restraint at both ends of the weld seam (compare Figs. 2b and 3). Hence, the results of restraint intensity determination are in very good accordance (see Table 1). Moreover, these values are in the scope of typical values in high-strength steel fabrication according to [19].

2.2 Welding experiments

The slot specimens were used to perform multilayer GMA weld tests in comparison to welding experiment at free shrinking specimens (see Figs. 4 and 5). Plates of high-strength quenched and tempered fine-grained structural steel S960QL (EN 10025-6 [20]) with a thickness of 20 mm were used. Welding was performed with a similar high-strength solid wire according to ISO 16834-A [21]. The chemical compositions and mechanical properties are shown in Table 2. In both test setups, the groove angle was varied. For the narrow seam geometry, a modified spray arc welding process was applied

in all weld runs [14]. The 45° V-type seam geometry was welded with a conventional GMAW process. The welding parameters are given in Table 3. The measured cooling times $\Delta t_{8/5}$ are between 6 and 8 s, which is within the recommended working range for this material. Hence, the mechanical-technological properties tested in the free shrinking specimens were in accordance to the standard requirements.

Displacements and strains which occur in the vicinity of the restrained weld seam due to local heat input and while cooling were detected with the DIC system (see Fig. 5). These measurements were performed at certain time and temperature steps while welding and cooling of the slot specimens. A stochastic greyscale value pattern was applied at one side of the weld vicinity (see Figs. 4 and 5). The stereo camera optic of the ARAMIS system allowed the analysis of the spatial displacement of each point on the stochastic pattern.

Temperature measurements were conducted using thermocouples (type-K) attached 10 mm adjacent to the weld. The working temperature was measured on the weld seam. $\Delta t_{8/5}$-cooling times were determined at the weld surface using a two-colour pyrometer (measuring range, 350 to 1300 °C). With a thermographic camera, the temperature field was observed.

Local residual stresses were analysed by means of X-ray diffraction (XRD) using the $\sin^2\psi$ method as in [9–11] with 5 to 7 ψ steps between 0° and $\pm 45°$ (10 to 20 s each step; CrKα, power, 30 kV at 6.7 mA). The measurements were taken out with a 2-mm colimator along the specimen centre line ($x = 0$ mm) on the surface of the base material, HAZ and weld metal. The measuring point density was from 1 to 10 mm,

Table 1 Comparison of restraint intensity determination

Seam geometry	Introduced load F_y in kN (at $p = 100$ N mm^{-2})	Average widening $2\Delta y$ in mm	Average restraint intensity R_{Fy} in kN (mm mm)$^{-1}$
V-type weld (numerical)	400.0	0.204	9.8
Square weld (numerical)	400.0	0.198	10.1
Square weld (experimental)	115.5	0.058	10.1

Fig. 4 In situ analyses of the temperatures and stress-strain fields adjacent to the weld, while preheating, welding and cooling, local residual stress analyses via XRD [5]

depending on the residual stress gradient. The analysis was primarily focussed on transverse residual stresses to investigate the superposition of local and global stresses and since restraint was varied in transverse direction (see Fig. 4).

In recent studies at BAM, also welding experiments with a unique 2-MN testing facility were performed [5, 8, 9, 12–14, 22]. Details of this testing facility and weld tests are given in [14]. In the 2-MN testing facility, specimens are hydraulically clamped into a three-dimensional operating test frame. The test frame consists of a hydraulic cylinder system with three piston rods. Hence, global lateral and angular distortions are restrained and the reaction forces, moments and stress could be measured synchronously while preheating, welding and cooling of the specimen. After cooling, at room temperature analyses of the superimposing local restraint stresses and the global stresses on the top surface of the welded specimen by means of XRD directly within the testing facility are enabled. This allowed a comparison with the results of the aforementioned analysis using free shrinking and slot specimens and a further discussion.

3 Results and discussion

3.1 Global strains and stresses

In Fig. 6, contour plots of the global displacement adjacent to the weld in transverse direction $-\Delta y(x,y)$ for the whole welding procedure of weld test no. 3 are shown. While local preheating of the weld seam, the thermal expansion causes a major displacement off the seam. After root welding, shrinkage of the weld produces a local movement of the weld vicinity towards the weld seam. With each weld sequence, the displacement off the seam in farer regions of the weld increases. In the weld vicinity, shrinkage and displacement towards the weld seam intensify. Subsequent cooling after cap weld pass causes a shifting of the complete measured pattern towards the weld due to the transverse shrinkage, which reaches a maximum at room temperature. The greatest displacement of approx. $-\Delta y = 0.22$ mm is revealed in the area near the specimen centre line ($x = 0$) adjacent to the weld seam. Towards the ends of the weld seam, displacement decreases due to comparable higher restraints in these areas (see Figs. 2 and 3).
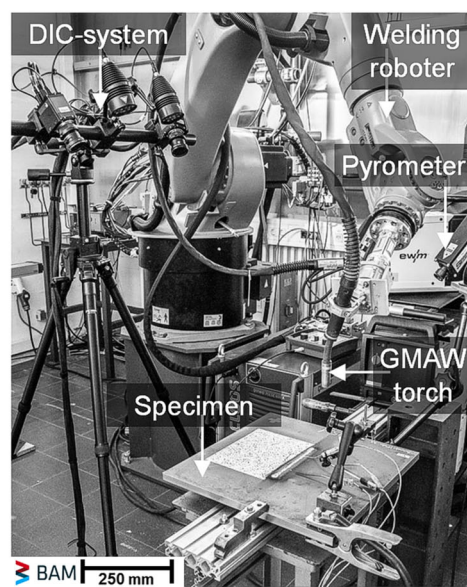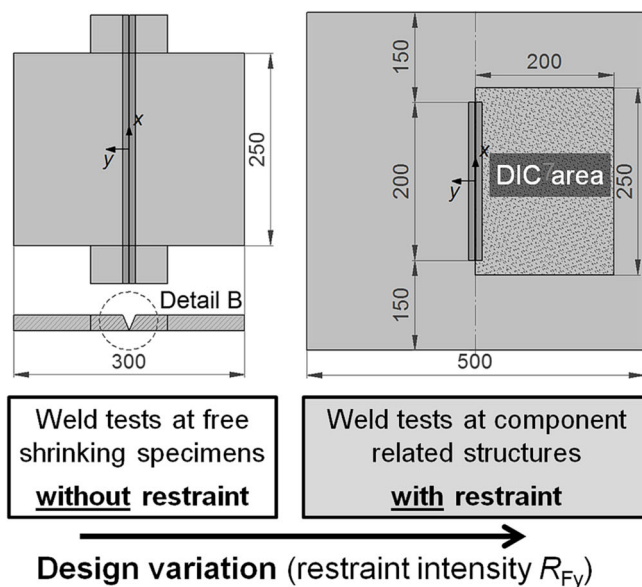

Fig. 5 Geometry of the free shrinking and slot specimen, test setup of the weld tests [5]

Table 2 Chemical compositions (FES, Fe balanced) and mechanical properties of the test materials

Element in %	C	Si	Mn	Cr	Mo	Ni	V	Nb	Ti
S960QL, base material	0.16	0.23	1.24	0.20	0.61	0.05	0.040	0.015	0.003
G 89 6M21 Mn4Ni2CrMo, filler material	0.08	0.87	1.84	0.35	0.57	2.23	0.005	–	0.070
Property	$R_{p0.2}$ in MPa	R_m in MPa	A_5 in %		Av in J at -40 °C			HV10	
S960QL (mechanical testing)	1035	1050	17		96			332 ± 8	
G 89 (producer testing report)	938	980	15		62			354 ± 7	

$-\Delta y_\mathrm{m}(t)$ and $\varepsilon_\mathrm{y,m}(t)$ graphs as mean values, measured with the DIC system 10 mm adjacent to the weld flank ($y = 20$ mm), and temperature $T(t)$ are presented in Fig. 7 for test no. 3. In accordance with Fig. 6, preheating, cooling to interpass and to room temperature cause transverse displacements towards the weld seam. Shrinkage is interrupted by phases, in which the heat input of the next weld run leads to a transient thermal expansion. Therefore, strain increases while heat input occurs and decreases while weld cools to interpass temperature. The maximum strain of $\varepsilon_\mathrm{y,m,max} = 0.14\%$ is observable after cap bead welding. Due to shrinkage while cooling, the strain decreases continuously and reaches a remaining strain at the weld vicinity ($y = 20$ mm) of about $\varepsilon_\mathrm{y,m,end} = 0.04\%$ at room temperature.

By comparison of average strains measured next to weld $\varepsilon_\mathrm{y,m}(t)$ of the conventional weld (test no. 3, compare Table 3) and the modified weld with a narrow weld groove (weld test no. 4), two qualitatively equal graphs are exposed (see Fig. 8). Quantitative differences reveal for the total welding time. The lower amount of weld runs for the narrow groove weld leads to shorter welding time. Although the strain level while welding is more or less equal for both processes, the lower total heat input and volume of inserted weld metal for the modified weld lead to significant lower strains $\varepsilon_\mathrm{y,m,end}$ remaining after cooling to ambient temperature.

This is the consequence of the higher number of weld runs needed for the conventional weld (conv. weld: 7 passes, mod. weld: 4 passes, compare Table 3) and a higher eccentricity of the weld in connection with a higher amount of weld runs which had to be inserted asymmetrically into the weld seam. All this causes an increased thermal expansion of about $\Delta\varepsilon_\mathrm{y} = 0.02\%$ at the top of the specimen, which cannot be compensated during temperature equalisation.

Hence, the global strain field $\varepsilon_\mathrm{y}(x,y)$ after subsequent cooling to ambient temperature of the modified weld (Fig. 9b) shows significantly reduced values compared to the conventional weld (Fig. 9a), especially in the area around the weld centre line ($x = 0$ mm). In the areas at the weld seam ends ($x = \pm(100$ to $125)$ mm), higher negative strains occur in the modified weld. In accordance with the strain fields, in Fig. 9c, d, the stress fields of both welds are shown. The stresses were calculated with the DIC system based on the strain measurements, the plate thickness and elastic constants (Young's modulus $E_\mathrm{M} = 215$ GPa, Poisson's ratio $\nu = 0.3$). The weld seam ends of the narrow weld reveal higher transverse compressive stresses. Particularly in the areas near the weld ($y = (20$ to $50)$ mm), the tensile stresses due to welding are approx. 100 MPa higher in the conventional welds compared to those in the narrow groove welds due to the higher restrained transverse shrinkage (compare Fig. 8).

3.2 Local stress analysis

The XRD measurements transverse to the weld direction along the centre line of the specimens ($x = 0$ mm, compare Fig. 9c and d) are shown in Fig. 10 as residual stress

Table 3 Welding parameters and variation of seam geometry and restraint condition

Seam geometry	Welding current in A	Welding voltage in V	Welding speed in mm min^{-1}	Wire feed speed in m min^{-1}	Welding parameters	Working temperature $T_\mathrm{p/i}$ in °C	Heat input in kJ mm^{-1}
V-type, 45°	265 ± 10	26.5 ± 0.1	330	8.7	Conv.	100	1.3
V-type, 30°	320 ± 10	28.7 ± 0.1	400 to 420	11	Mod.		
Test no.				1	2	3	4
Groove angle		α	in °	45	30	45	30
Welding parameters		–	–	Conv.	Mod.	Conv.	Mod.
Restraint intensity		R_Fy	in kN (mm mm)$^{-1}$	0[a]	0[a]	10[b]	10[b]

Welding parameters of the power source: Conv., transitional arc; Mod., modified spray arc

[a] Free shrinking weld test
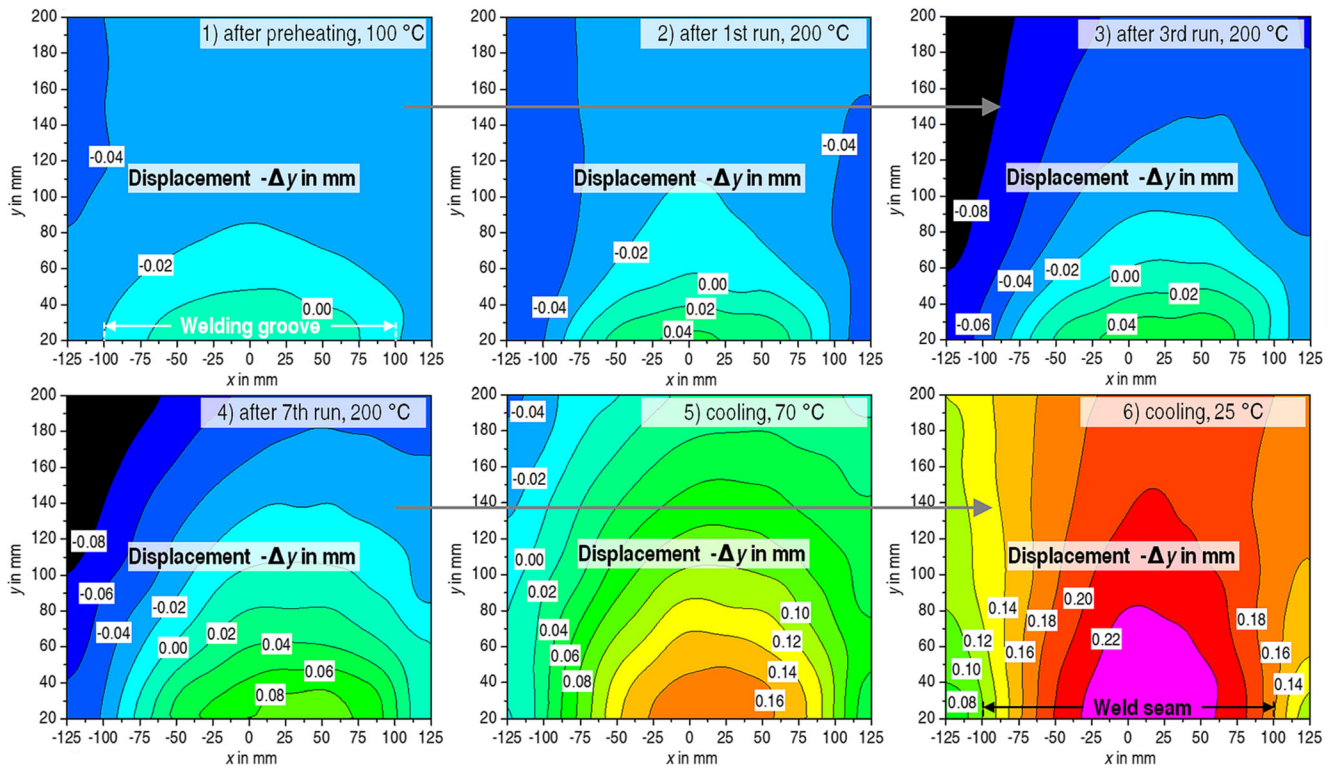
[b] Self-restrained weld test (slot weld)

Fig. 6 Contour plots of transverse displacement $-\Delta y(x,y)$ at certain phases of welding procedure (test no. 3) [5]

distributions $\sigma^{rs}{}_y(y)$ of all four weld tests according to Table 3. Both XRD (see Fig. 10) and DIC analyses (Fig. 9) revealed comparable results regarding welding stress level in compliance with the restraint intensity determinations [5].

All graphs exhibit qualitative equal, typical residual stress profiles for steel welds with an undergoing phase transformation according to common concepts [11]. The microstructure of the welds as well as the influence of solid state phase transformation while cooling on the local and global welding stresses and loads is widely discussed in [5, 9–11, 15]. Along with material properties, heat control and cooling conditions while

welding may have a strong effect on the residual stress evolution. In this study, the same materials and constant heat control parameters were used to mask these effects.

By comparison of the residual stresses in Fig. 10, a broader stress profile reveals for the wider weld groove ($\alpha = 45°$). Maximum residual stresses are typically on the weld metal surface. The weld interface is affected by high residual stress gradients. Secondary maxima of the residual stresses occur in the HAZ. In the free shrinking specimens, which were welded and measured without restraint, the stresses decrease to the level of the initial state towards the unaffected base material.

Fig. 7 $-\Delta y_m(t)-$ and $\varepsilon_{y,m}(t)$ graphs and temperature $T(t)$ measured in test no. 3; mean values measured at $y = 20$ mm adjacent to the weld seam [22]
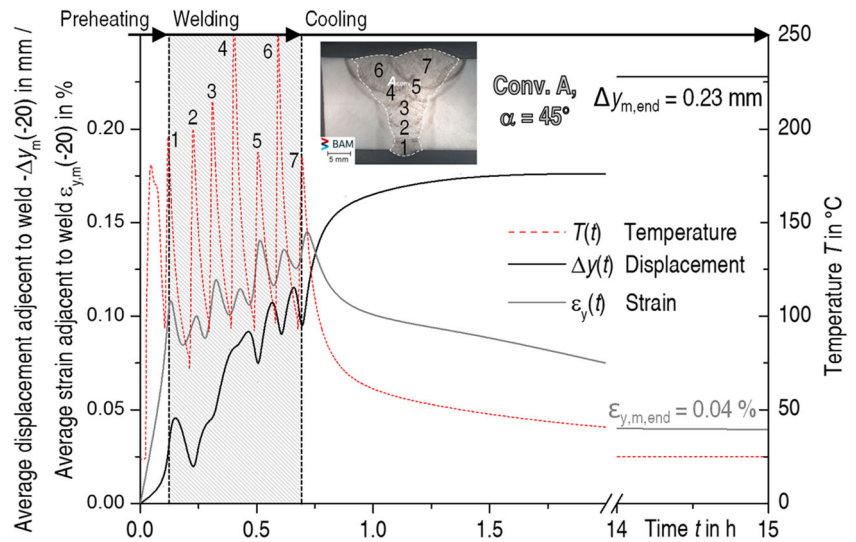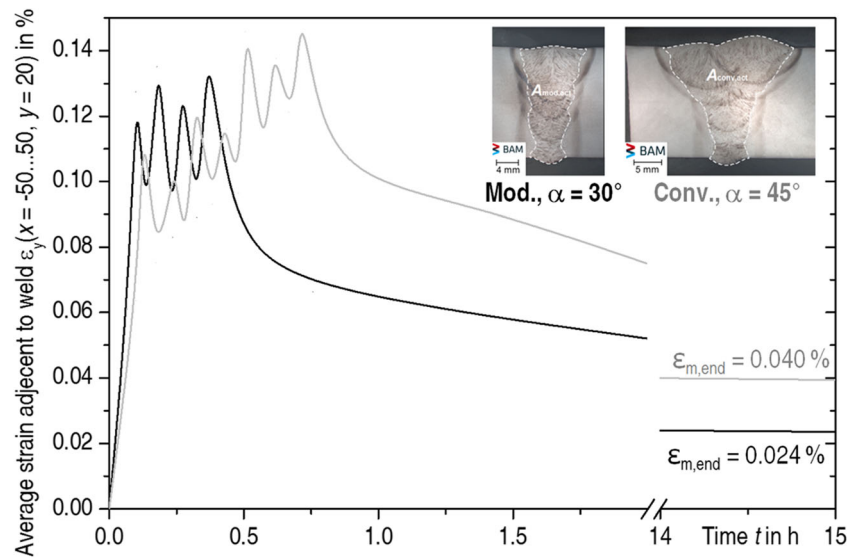
Fig. 8 $\varepsilon_{y,m}(t)$ graphs for two weld tests with different weld geometries (weld test nos. 3 and 4) [22]

Note that the base material surface was blast cleaned and reveals residual stresses of about −160 MPa. Hence, a superposition of the reaction stresses and the local restraint stresses in the weld area is revealed for the specimen welded and measured under restraint. In the base material, the stress level is elevated by approx. 50 to 150 MPa in the restrained slot specimens. According to the DIC analyses, the reaction stresses in the conventional weld are significantly higher, which is evident in the areas nearby the weld seam flank or HAZ, respectively. At the weld metal of the modified welds, higher tensile residual stresses of the amount of 60% of $R_{p0.2}$ of the weld metal are obviously almost independent of the restraint intensity, which is due to a deeper weld penetration [5, 14]. The lowest residual stresses in weld metal can be

Fig. 9 $\varepsilon_{y,m}(t)$ graphs (**a** and **b**) and $\Delta_y(x,y)$ graphs (**c** and **d**) for two weld tests with various weld geometries (weld test nos. 3 and 4) after cooling to room temperature [22]
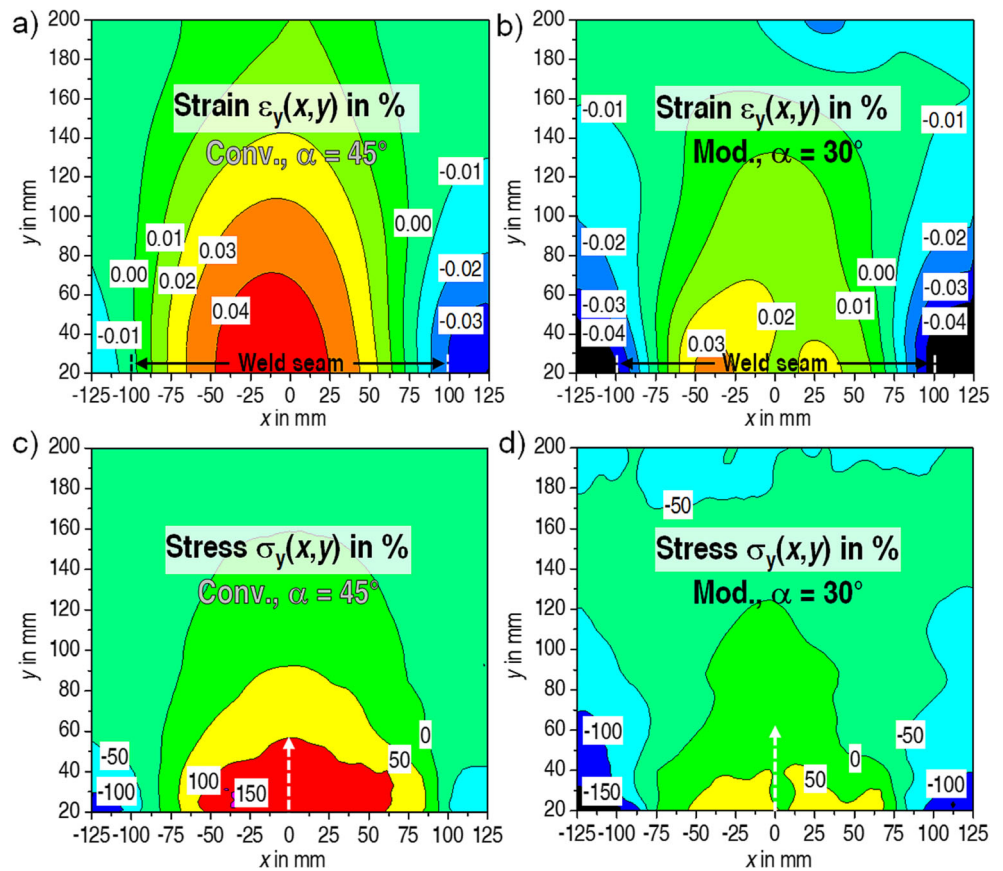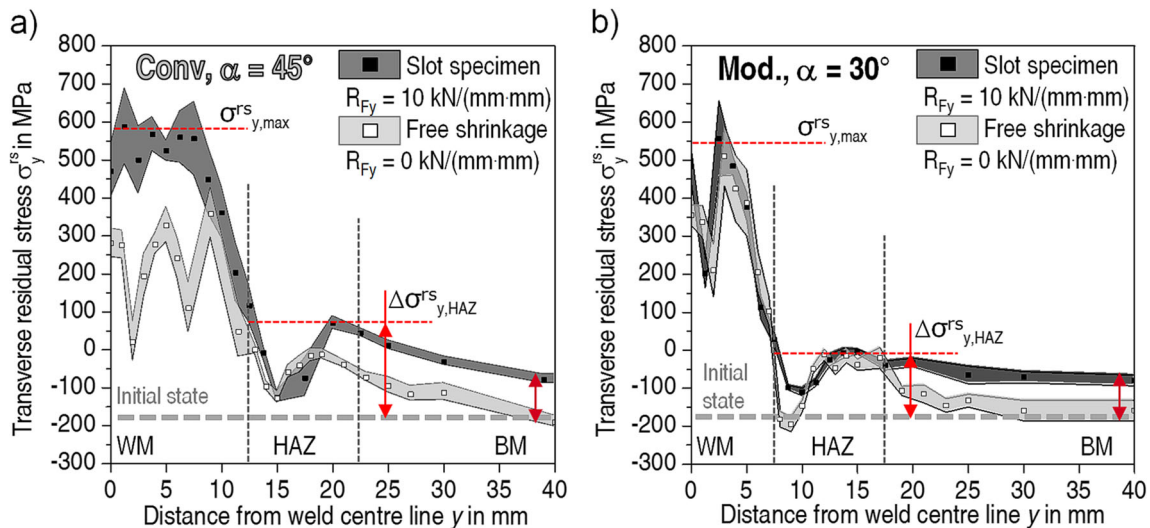
Fig. 10 $\sigma^{rs}_y(y)$ distributions for **a** conventional welds (test nos. 1 and 3) and **b** modified welds (test nos. 2 and 4), welded and measured under different restraint conditions [5]

found in the conventional weld of the free shrinking specimen (weld test no. 1). However, the maximum tensile residual stresses in the conventional welds ($\sigma^{rs}_{y,max}$) grow with increasing restraint intensity up to 70% of $R_{p0.2}$.

In general, especially if occurring in the HAZ, high residual stresses are detrimental since a critical microstructure and, therefore, significantly degraded mechanical properties may be present. From the DIC and XRD measurements, it could be stated that the narrow weld groove in context with the selected process conditions (welding process, heat control) has a positive effect on the loads and stresses especially in the vicinity of the weld. For a safe welding manufacturing and for a minimal risk of premature failure, such findings should be taken into account particularly with regard to severe restraint conditions.

3.3 Comparison with recent studies

However, residual stress analyses of the slot specimens (see Fig. 10) revealed some divergent results compared to earlier studies that were carried out with special testing facilities [5, 8, 9, 12–14, 22]. Hence, in Fig. 11, residual stress distributions of conventional welds with the same materials and welding parameters as weld test nos. 1 and 3 (see Table 3) are presented. These welds were conducted at the 2-MN testing facility under two various restraint conditions [5, 14]. The restraint conditions were varied by means of different weld seam lengths (L_w = 100 and 200 mm).

In comparison with Fig. 10a, considerably lower residual stresses are revealed at the surface of the weld metal. This is due to the lower restraint intensity transverse to the weld direction, which is 30 and 40% of the slot specimen, respectively. In contrast, the residual stress levels in the HAZ of both specimens

welded in the testing facility are significantly higher. According to [14, 22, 23], these high residual stress levels in the HAZ are due to increased bending moments and, therefore, bending stresses occurring in the weld seams of the specimens that were welded conventionally using a larger groove angle of $\alpha = 45°$. Since the bending stresses are a result of a restrained angular distortion, the higher residual stresses in the HAZ should be attributed to a higher bending restraint intensity [18].

Hence, Fig. 12 shows the determination of the bending restraint intensity R_{Mx} of the different test setups of the 2-MN testing facility and the slot welds. The comparably longer lever arms of the testing facility involve a bending restraint
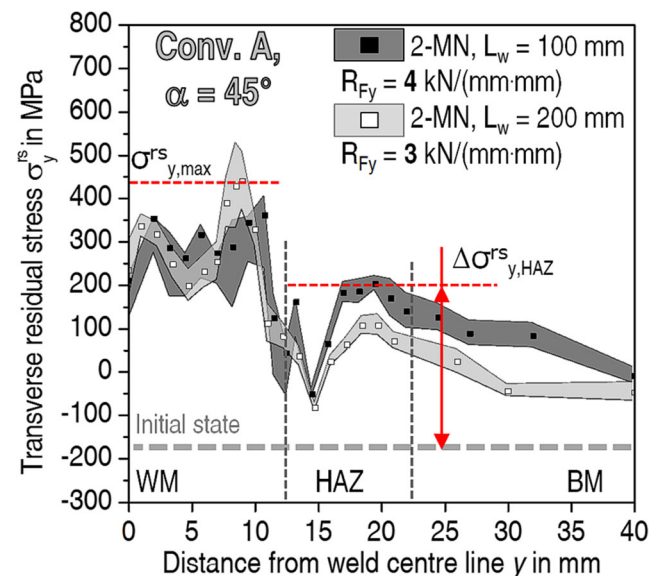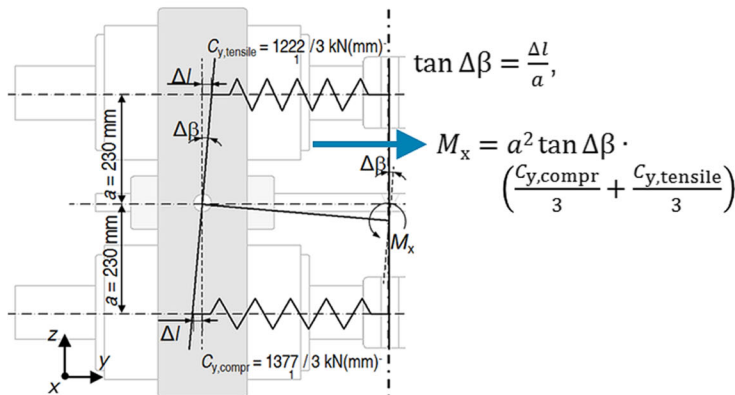

Fig. 11 $\sigma^{rs}_y(y)$ distributions for conventional welds in the 2-MN testing facility for two various restraint conditions [5, 14]

Bending restraint intensity: $R_{Mx} = \dfrac{M_x}{2\Delta\beta \cdot L_S}$, suspension due to:
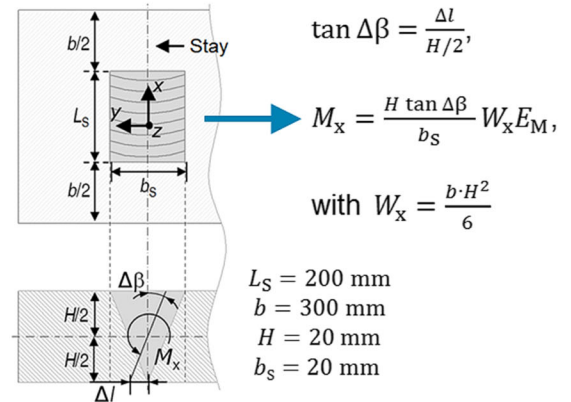
Stiffness of the 2-MN-testing facility
(piston rods top right side, lower right side)

$C_{y,\text{tensile}} = 1222\ /3\ \text{kN(mm)}$

$a = 230\ \text{mm}$

$a = 230\ \text{mm}$

$C_{y,\text{compr}} = 1377\ /3\ \text{kN(mm)}$

$\tan\Delta\beta = \dfrac{\Delta l}{a},$

$M_x = a^2 \tan\Delta\beta \cdot \left(\dfrac{C_{y,\text{compr}}}{3} + \dfrac{C_{y,\text{tensile}}}{3} \right)$

Section modulus of the stay
(adjacent to end of seam)

$\tan\Delta\beta = \dfrac{\Delta l}{H/2},$

$M_x = \dfrac{H \tan\Delta\beta}{b_S} W_x E_M,$

with $W_x = \dfrac{b \cdot H^2}{6}$

$L_S = 200\ \text{mm}$
$b = 300\ \text{mm}$
$H = 20\ \text{mm}$
$b_S = 20\ \text{mm}$

for $L_S = 100\ \text{mm}$: $\boldsymbol{R_{Mx,2MN100}} = \dfrac{\textbf{16,0 kNm}}{\textbf{°·mm}}$

for $L_S = 200\ \text{mm}$: $\boldsymbol{R_{Mx,2MN200}} = \dfrac{\textbf{8,0 kNm}}{\textbf{°·mm}}$

$\boldsymbol{R_{Mx,Slot}} = \dfrac{\textbf{0,7 kNm}}{\textbf{°·mm}}$

Fig. 12 Analytical determination of bending restraint intensities for the 2-MN testing facility and the slot weld test setup (L_S weld length, b_S weld width, ß angular distortion, C spring rigidity, H plate thickness, W_x section modulus) [5]

that revealed to be more than eight times higher than that in the slot weld. The reduction of the weld length from $L_S = 200$ to 100 mm of the specimen in the 2-MN testing facility would additionally double the bending restraint to $R_{Mx} = 16$ kNm $(°·mm)^{-1}$ whereas the restraint intensity transverse to the weld increases merely from $R_{Fy} = 3$ to 4 kN (mm mm)$^{-1}$.

Finally, Fig. 13a shows that the transverse residual stress level in the weld metal under equal material and welding parameters is a linear function of the restraint intensity transverse to the weld seam. In contrast, the occurrence of bending stresses due to hindered angular distortion induces a linear correlation between the residual stress levels in the HAZ and the bending restraint intensity (see Fig. 13b). Thus, it should be noted that especially high bending restraints might lead to crack critical tensile stresses in the vicinity of high-strength steel welds if inadequate welding or heat control parameters are applied.
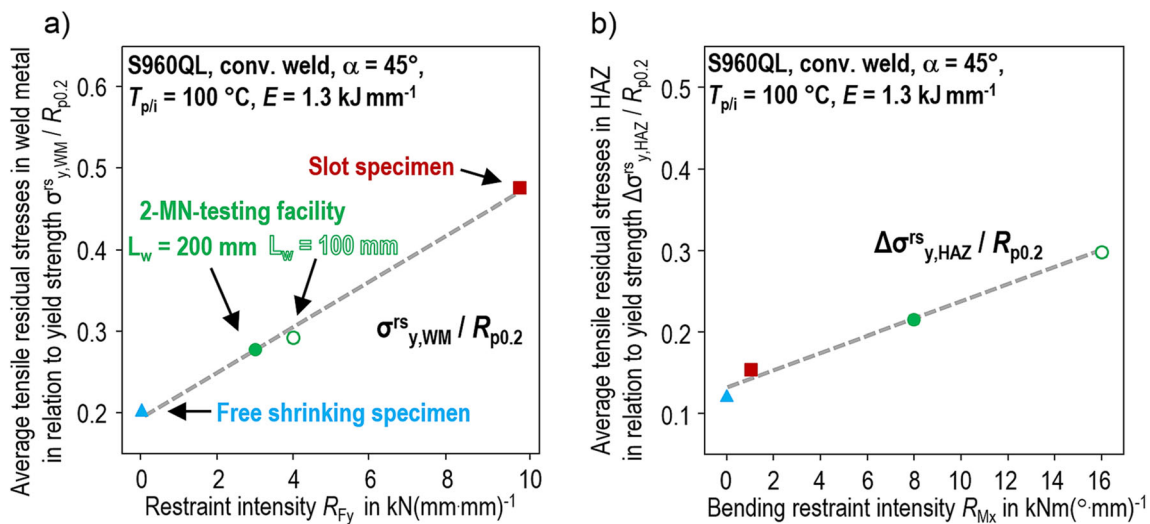

Fig. 13 **a** Residual stress level in the weld metal $\sigma^{rs}_{y,wm}/R_{p0.2}$ of the conventional welds vs. restraint intensity transverse to the weld R_{Fy}, σ. **b** Residual stress level in the HAZ $\Delta\sigma^{rs}_{y,HAZ}/R_{p0.2}$ of the conventional welds vs. bending restraint intensities R_{Mx} [5]

4 Conclusions

Derived from real high-strength structural steel components in the mobile crane industry, a specimen geometry was selected to undertake weld tests under defined restraint conditions. The restraint intensity of the test setup was analysed and multilayer GMA welds were performed with two different weld geometries and welding parameter sets at these component-related specimens and at free shrinking specimens from S960QL. With in situ DIC, temperature and XRD measurements, the resulting welding stresses were analysed and compared with results from recent studies. From this work, the following conclusions can be draw:

1. The numerical and experimental analysed restraint intensities of the slot specimens are in very good accordance and in the scope of typical high-strength steel weldments.
2. In the self-restrained slot specimens using a DIC system, in situ measurements of the induced strain were carried out and the strain and stress fields were analysed. As shown in recent analyses, the weld seam with the smaller groove angle causes significantly decreased strains and stresses in the vicinity of the weld.
3. A local analysis of stress superposition using XRD in the weld seam area revealed a high effect of the restraint condition on the transverse residual stresses, especially in the weld metal and the HAZ of the welds, which were prepared with a larger groove angle. Using same material and welding conditions, the residual stress level in the weld metal correlates with the transverse shrinkage restraint.
4. Results of recent studies of welds in a unique testing machine of the BAM [5, 14, 22] revealed that local transverse residual stresses in the HAZ are higher in the specimens despite a lower restraint intensity in the transverse direction. An analytical estimation of bending restraint intensities in each test setup showed values up to 16 times higher in the 2-MN testing facility. Hence, it could be clarified that welding induced bending stresses increase with the bending restraint and cause higher local residual stresses in the HAZ. This was shown by a correlation of the stress level in the HAZ and the bending restraint intensity.
5. Slender seam geometries and adequate process conditions may lead to considerably lower bending stresses and tensile residual stresses in the HAZ, despite severe restraint conditions. This is important to consider while welding high-strength steel structures, since detrimental microstructures and degraded mechanical properties may be evident in the HAZ, involving a higher susceptibility for premature failures if tensile stresses occur.

These results should help in deriving optimal heat control parameters for certain weld tasks in high-strength steel fabrication in order to reduce welding loads, which beneficially affects the economic application and exploitation of the potential of high-strength structural steel.

References

1. Guenther H-P (2005) Use and application of high-performance steels for steel structures. IABSE IVBH, Zürich
2. Adamczyk J (2006) Development of the microalloyed constructional steels. J Achiev Mater Manuf Eng 14:9–20
3. Leggatt RH (2008) Residual stresses in welded structures. Press Vessel Pip 85:144–151. https://doi.org/10.1016/j.ijpvp.2007.10.004
4. Dong P, Hong JK, Bouchard PJ (2005) Analysis of residual stresses at weld repairs. Int J Press Vessel Pip 82:258–269. https://doi.org/10.1016/j.ijpvp.2004.08.004
5. Schroepfer D (2017) Adaptierte Wärmeführung zur Optimierung schweißbedingter Beanspruchungen und Eigenschaften höherfester Verbindungen. Dissertation, OVGU Magdeburg
6. (2001) DIN EN 1011-2: Welding—recommendation for welding of metallic materials—part 2: arc welding of ferritic steels
7. (2010) Eurocode 3: design of steel structures (EN 1993)
8. Schroepfer D, Kannengiesser T, Kromm A (2014) Influence of heat control on welding stresses in multilayer-component welds of high-strength steel S960QL. Adv Mater Res 996:475–480. https://doi.org/10.4028/www.scientific.net/AMR.996.475
9. Schroepfer D, Kromm A, Kannengiesser T (2015) Improving welding stresses by filler metal and heat control selection in component-related butt joints of high-strength steel. Weld World 58:455–464. https://doi.org/10.1007/s40194-014-0219-7
10. Nitschke-Pagel T, Wohlfahrt H (2002) Residual stresses in welded joints—sources and consequences. Mater Sci Forum 404–407:215–226. https://doi.org/10.4028/www.scientific.net/MSF.404-407.215
11. Nitschke-Pagel T, Wohlfahrt H (1991) The generation of residual stresses due to joining processes. In: Hauk V, Hougardy H, Macherauch E (eds) Residual Stresses: Measurement, Calculation, Evaluation: Proceedings of a Symposium 1990. DGM Informationsgesellschaft mbH, pp 121–133
12. Lausch T, Kannengiesser T, Schmitz-Niederau M (2013) Multi-axial load analysis of thick-walled component welds made of 13CrMoV9-10. J Mater Process Technol 213:1234–1240. https://doi.org/10.1016/j.jmatprotec.2013.01.008
13. Schroepfer D, Kromm A, Kannengiesser T (2016) Engineering approach to assess residual stresses in welded components. Weld World 61:91–106. https://doi.org/10.1007/s40194-016-0394-9
14. Schroepfer D, Kromm A, Kannengiesser T (2017) Optimization of welding loads with narrow groove and application of modified spray arc process. Weld World 61:1077–1087. https://doi.org/10.1007/s40194-017-0484-3

15. Schroepfer D, Kannengiesser T (2016) Stress build-up in HSLA steel welds due to material behaviour. J Mater Process Technol 227:49–58. https://doi.org/10.1016/j.jmatprotec.2015.08.003

16. Schwenk C, Kannengiesser T, Rethmeier M (2009) Restraint conditions and welding residual stresses in self-restrained cold cracking tests. In: Trends Weld. Res. Proc. 8th Int. Conf. June, 2008, Callaw. Gard. Resort, Pine Mt. Georg. USA. ASM International, pp 766–773. https://doi.org/10.1361/cp2008twr766

17. Kannengiesser T, Gruender K-P (2013) Handbook of Technical Diagnostics. Appl Struct Syst. pp 69–108. https://doi.org/10.1007/978-3-642-25850-3_5

18. Satoh K, Nakajima H, Toyosada M (1972) Restraint intensity of weld joints in the structural members consisting of plates and stiffeners, IIW-Doc X-660-72. Welding Research Institute, Osaka University, Hitachi Shipbuilding & Engineering Co., Osaka, Japan

19. Satoh K, Ueda Y, Matsui S et al (1977) Japanese studies on structural restraint severity in relation to weld cracking. Weld World 15:155–189

20. (2011) EN 10025-6: Hot rolled products of structural steels—part 6: technical delivery conditions for flat products of high yield strength structural steels in the quenched and tempered conditions

21. (2012) EN ISO 16834: Welding consumables—wire electrodes, wires, rods and deposits for gas shielded arc welding of high strength steels—classification

22. Schroepfer D, Flohr K, Kromm A, Kannengiesser T (2017) Multi-axial analyses of welding stresses in high-strength steel welds. In: Mater. Res. Proceedings, Residual Stress. 2016 ICRS-10. Materials Research Forum, Sydney, Australia, pp 205–210. https://doi.org/10.21741/9781945291173-35

23. Rhode M, Kromm A, Kannengiesser T (2012) Residual stresses in multi-layer component welds. In: DebRoy T, Koseki T, David SA et al (eds) Proc. 9th Int. Conf. Trends Weld. Res. ASM International, Chicago, pp 48–54. https://doi.org/10.21741/9781945291173-35